



Characterization of ANGPTL4 function in macrophages and adipocytes using *Angptl4*-knockout and *Angptl4*-hypomorphic mice^S

Antwi-Boasiako Oteng,^{1,*} Philip M. M. Ruppert,^{1,*} Lily Boutens,^{*,†} Wieneke Dijk,^{2,*} Xanthe A. M. H. van Dierendonck,^{*,†} Gunilla Olivecrona,[§] Rinke Stienstra,^{*,†} and Sander Kersten^{3,*}

Nutrition, Metabolism and Genomics Group,^{*} Division of Human Nutrition and Health, Wageningen University, Wageningen, The Netherlands; Department of Internal Medicine,[†] Radboud University Medical Center, Nijmegen, The Netherlands; and Department of Medical Biosciences/Physiological Chemistry,[§] Umeå University, Umeå, Sweden

Abstract Angiopoietin-like protein (ANGPTL)4 regulates plasma lipids, making it an attractive target for correcting dyslipidemia. However, ANGPTL4 inactivation in mice fed a high fat diet causes chylous ascites, an acute-phase response, and mesenteric lymphadenopathy. Here, we studied the role of ANGPTL4 in lipid uptake in macrophages and in the above-mentioned pathologies using *Angptl4*-hypomorphic and *Angptl4*^{-/-} mice. *Angptl4* expression in peritoneal and bone marrow-derived macrophages was highly induced by lipids. Recombinant ANGPTL4 decreased lipid uptake in macrophages, whereas deficiency of ANGPTL4 increased lipid uptake, upregulated lipid-induced genes, and increased respiration. ANGPTL4 deficiency did not alter LPL protein levels in macrophages. *Angptl4*-hypomorphic mice with partial expression of a truncated N-terminal ANGPTL4 exhibited reduced fasting plasma triglyceride, cholesterol, and NEFAs, strongly resembling *Angptl4*^{-/-} mice. However, during high fat feeding, *Angptl4*-hypomorphic mice showed markedly delayed and attenuated elevation in plasma serum amyloid A and much milder chylous ascites than *Angptl4*^{-/-} mice, despite similar abundance of lipid-laden giant cells in mesenteric lymph nodes. **In conclusion, ANGPTL4 deficiency increases lipid uptake and respiration in macrophages without affecting LPL protein levels. Compared with the absence of ANGPTL4, low levels of N-terminal ANGPTL4 mitigate the development of chylous ascites and an acute-phase response in mice.**—Oteng, A-B., P. M. M. Ruppert, L. Boutens, W. Dijk, X. A. M. H. van Dierendonck, G. Olivecrona, R. Stienstra, and S. Kersten. **Characterization of ANGPTL4 function in macrophages and adipocytes using *Angptl4*-knockout and *Angptl4*-hypomorphic mice.** *J. Lipid Res.* 2019. 60: 1741–1754.

Supplementary key words angiopoietin-like protein 4 • lipoprotein lipase • dyslipidemia • macrophage foam cells • inflammation • glucose homeostasis

This work was supported by the Graduate School Voeding, Levensmiddelen-technologie, Agro-Biotechnologie en Gezondheid (VLAG) (Wageningen University), and CVON ENERGISE Grant CVON2014-02. The authors declare that there are no conflicts of interest associated with this work.

Manuscript received 21 March 2019 and in revised form 13 August 2019.

Published, *JLR Papers in Press*, August 13, 2019
DOI <https://doi.org/10.1194/jlr.M094128>

Copyright © 2019 Oteng et al. Published under exclusive license by The American Society for Biochemistry and Molecular Biology, Inc.

This article is available online at <http://www.jlr.org>

Elevated plasma triglyceride levels are increasingly considered as an independent risk factor for cardiovascular diseases (1–3). Triglycerides circulate in the blood in two major forms: as chylomicrons carrying the dietary triglycerides and as very low density lipoproteins carrying endogenously produced triglycerides (4). The clearance of plasma triglycerides is primarily mediated by the action of LPL. This secretory enzyme is produced by parenchymal cells of fat tissue, skeletal muscle, and heart, as well as by macrophages. With the help of the endothelial protein, glycosylphosphatidylinositol-anchored HDL binding protein 1 (GPIHBP1), LPL is transferred from the surface of the sub-endothelial myocytes and adipocytes to the luminal side of the capillary endothelium. There, LPL hydrolyzes the triglycerides contained in the triglyceride-rich lipoproteins to release fatty acids for uptake by the underlying tissues (5–8). The activity of LPL is regulated posttranslationally by numerous factors, many of which are produced in the liver, including several apolipoproteins. In addition, LPL activity is governed by several members of the family of angiopoietin-like proteins (ANGPTLs): ANGPTL3 (9), ANGPTL4 (10–12), and ANGPTL8 (13–15).

ANGPTL3 is produced in the liver and cooperates with ANGPTL8 to inhibit LPL activity in peripheral tissues

Abbreviations: ANGPTL, angiopoietin-like protein; BMDM, bone marrow-derived macrophage; FCCP, carbonyl cyanide 4-(trifluoromethoxy)phenylhydrazide; OCR, oxygen consumption rate; PS, penicillin/streptomycin; SAA, serum amyloid A.

The data discussed in this publication have been deposited in NCBI's Gene Expression Omnibus (Oteng et al., 2019) and are accessible through GEO Series accession number GSE136240; (<http://www.ncbi.nlm.nih.gov/geo/query/acc.cgi?acc=GSE136240>).

¹A-B. Oteng and P. M. M. Ruppert contributed equally to this work.

²Present address of W. Dijk: L'Institut du Thorax, U1087, INSERM, Nantes, France.

³To whom correspondence should be addressed.

e-mail: sander.kersten@wur.nl

^S The online version of this article (available at <http://www.jlr.org>) contains a supplement.

(15–17). The role of ANGPTL3/ANGPTL8 in LPL regulation is particularly important in the fed state (18). By contrast, ANGPTL4 mainly plays a role in LPL regulation in the fasted state (19). Individuals who carry an inactive variant of ANGPTL4 exhibit lower levels of circulating triglycerides and have decreased odds of developing coronary heart disease (20, 21). In mice, overexpression of ANGPTL4 potentially represses LPL activity and leads to hypertriglyceridemia, whereas deletion of ANGPTL4 stimulates LPL activity and drastically reduces plasma triglyceride levels (18, 22). In contrast to ANGPTL3, which functions as an endocrine factor, ANGPTL4 likely serves as a local regulator of LPL in tissues where LPL and ANGPTL4 are coproduced (23). Inhibition of LPL is mediated by the N-terminal coiled-coiled domain of ANGPTL4, causing the unfolding and inactivation of LPL, which may be accompanied by a change in the aggregation state of LPL (19, 24, 25). In adipocytes, ANGPTL4 promotes the cleavage and subsequent degradation of LPL, thereby preventing the delivery of LPL to the endothelial surface (26, 27). The important role of ANGPTL4 in governing plasma lipid levels in humans has made ANGPTL4 an attractive therapeutic target for correcting dyslipidemia and associated cardiovascular disorders.

However, we and others have shown that disabling ANGPTL4, via monoclonal antibody-mediated or genetic inactivation, leads to a highly pro-inflammatory and ultimately lethal phenotype in mice fed a high saturated fat diet (28, 29). This marked phenotype includes mesenteric lymphadenopathy, characterized by the presence of lipid-laden Touton giant cells in the mesenteric lymph nodes, as well as fibrinopurulent peritonitis, chylous ascites, and marked elevation of acute-phase proteins in plasma, such as serum amyloid A (SAA) and haptoglobin (29, 30). Accumulation of lipids in mesenteric lymph nodes was also observed in several female monkeys treated with an anti-ANGPTL4 antibody (21). Although there is so far no evidence pointing to the occurrence of abdominal lymphadenopathy in humans homozygous for an inactive ANGPTL4 variant (21), currently the therapeutic prospects of whole-body ANGPTL4 inactivation are not very favorable.

The deleterious effects of ANGPTL4 inactivation in mesenteric lymph nodes were previously attributed to the role of ANGPTL4 as LPL inhibitor in macrophages. Specifically, ANGPTL4 inactivation would increase LPL activity, leading to excessive lipid uptake in macrophages and a concomitant pro-inflammatory response (29). We have shown that recombinant ANGPTL4 represses lipid uptake into peritoneal macrophages incubated with chyle (29). However, whether endogenous ANGPTL4 suppresses lipid uptake into macrophages was not addressed. Accordingly, the first aim of this work was to examine the influence of endogenous ANGPTL4 on lipid uptake and utilization in macrophages and explore the underlying mechanisms.

The mouse model that revealed the effect of ANGPTL4 inactivation on mesenteric lymphadenopathy and other pathologies is a whole-body ANGPTL4 knockout model characterized by the deletion of exons 2 and 3 and part of intron 1, leading to the absence of ANGPTL4 protein (31).

Whether other and milder forms of genetic ANGPTL4 inactivation in mice provoke a similar phenotype upon feeding a high saturated fat diet is unclear. Accordingly, the second aim of this work was to further investigate the role of ANGPTL4 in the aforementioned pathologies using *Angptl4*-hypomorphic mice.

MATERIALS AND METHODS

Animal studies

Animal studies were performed in male purebred WT, *Angptl4*^{hyp}, and *Angptl4*^{-/-} mice. All mice were on the same C57Bl/6 background strain. The *Angptl4*^{hyp} mice were a kind donation from Dr. Nguan Soon Tan (Nanyang Technological University, Singapore). The *Angptl4*^{hyp} mice can also be classified as *Angptl4* knockout first mice (32), which upon stepwise crossing with mice expressing flippase recombinase and Cre recombinase can be used to generate a tissue-specific *Angptl4* knockout mouse model (33, 34). The sequence of the *Angptl4* construct is available online (https://www.i-dcc.org/imits/targ_rep/alleles/5215/escell-clone-genbank-file).

The animal studies were all carried out at the Centre for Small Animals, which is part of the Centralized Facilities for Animal Research at Wageningen University and Research (CARUS), and were approved by the Local Animal Ethics Committee of Wageningen University (AVD104002015236: 2016.W-0093.005, 2016.W-0093.007). Mice were maintained at 21°C and kept on a regular day-night cycle (lights on from 6:00 AM to 6:00 PM).

High fat diet intervention. Eleven- to 16-week-old mice (10 WT, 11 *Angptl4*^{hyp}, and 8 *Angptl4*^{-/-}) were fed a high fat diet containing 45 energy percent as triglycerides (D12451; Research Diets Inc., New Brunswick, NJ). The high fat feeding of the three groups of mice was not done in parallel. The *Angptl4*^{hyp} mice were run separately from the WT and *Angptl4*^{-/-} mice. After weeks 2 and 4 of the intervention, blood samples were collected to measure plasma SAA. After 20 weeks, blood was collected via orbital puncture under isoflurane anesthesia. Immediately thereafter, the mice were euthanized by cervical dislocation. Tissues were excised and immediately frozen in liquid nitrogen followed by storage at -80°C.

Fasting intervention. Mice were fed a standard chow diet after weaning. Mice were either kept on chow or fasted for 24 h and euthanized between 9:00 and 11:00 AM. Blood was collected via orbital puncture under isoflurane anesthesia. Immediately thereafter, the mice were euthanized by cervical dislocation. Tissues were excised and immediately frozen in liquid nitrogen followed by storage at -80°C.

Intraperitoneal glucose tolerance test. After 18 weeks of high fat diet, the mice were fasted for 5 h prior to the glucose tolerance test. The mice were injected intraperitoneally with glucose (1 g/kg body weight) (Baxter, Deerfield, IL). Blood samples from tail vein bleeding were tested for glucose levels at different time points following glucose injection using a GLUCOFIX Tech glucometer and glucose sensor test strips (Menarini Diagnostics, Valkenswaard, The Netherlands).

Histology

H&E staining was performed on the mesenteric lymph nodes. During the mouse sections, lymph nodes were isolated into plastic cassettes and immediately fixated in 4% paraformaldehyde. The

tissues were processed and embedded into paraffin blocks. Thin sections of the blocks were made at 5 μm using a microtome and placed onto Superfrost glass slides followed by overnight incubation at 37°C. The tissues were stained in Mayer hematoxylin solution for 10 min and in eosin for 10 s at room temperature with intermediate washings in ethanol. The tissues were allowed to dry at room temperature followed by imaging using a light microscope.

Quantification of plasma parameters

Blood samples were collected into EDTA-coated tubes and centrifuged at 4°C for 15 min at 12,879 *g*. Plasma was collected and stored at -80°C. ELISA kits were used to measure plasma serum amyloid (SAA) (Tridelta Development Ltd., Ireland) and haptoglobin (Abcam, Cambridge, UK) according to manufacturer's protocol. Measurement of plasma levels of triglycerides, NEFAs, and glycerol were performed using kits from HUMAN Diagnostics (Wiesbaden, Germany) according to manufacturer's protocol. Plasma levels of cholesterol and glucose were also measured using kits from Diasys Diagnostics Systems (Holzheim, Germany) according to manufacturer's protocol.

LPL activity measurements

LPL activity levels in epididymal white adipose tissues were measured in triplicate with a [³H]triolein-labeled lipid emulsion as previously described (35). Protein contents in homogenates of adipose tissue were measured using Markwell's modified Lowry method (36).

Cell culture

Bone marrow cells were isolated from femurs of WT or *Angptl4*^{-/-} mice following standard protocol and differentiated into macrophages [bone marrow-derived macrophages (BMDMs)] in 6–8 days in DMEM (Lonza, Verviers, Belgium) containing 10% FBS and 1% penicillin/streptomycin (PS) supplemented with 20% L929-conditioned medium. After 6–8 days, nonadherent cells were removed and adherent cells were washed and plated in 6-, 12-, or 48-well plates in DMEM/FBS/PS + 5% L929-conditioned medium. After 24 h, the cells were washed with PBS and treated. Peritoneal macrophages were obtained by infusion and subsequent collection of ice-cold PBS from the abdominal cavity and frozen directly or brought into culture in DMEM containing 10% FBS and 1% PS. RAW264.7 macrophages were cultured in DMEM containing 10% FBS and 1% PS. All cells were maintained in a humidified incubator at 37°C with 5% CO₂.

Inguinal white adipose tissue from three or four WT, *Angptl4*^{hyp}, and *Angptl4*^{-/-} mice was collected and placed in DMEM supplemented with 1% PS and 1% BSA (BSA; Sigma-Aldrich). Material was minced with scissors and digested in collagenase-containing medium [DMEM with 3.2 mM CaCl₂, 1.5 mg/ml collagenase type II (C6885; Sigma-Aldrich), 10% FBS, 0.5% BSA, and 15 mM HEPES] for 1 h at 37°C with occasional vortexing. Cells were filtered through a 100 μm cell strainer (Falcon) to remove remaining cell clumps and lymph nodes. The cell suspension subsequently was centrifuged at 229 *g* for 10 min and the pellet was resuspended in erythrocyte lysis buffer (155 mM NH₄Cl, 12 mM NaHCO₃, 0.1 mM EDTA). Upon incubation for 2 min at room temperature, cells were centrifuged at 129 *g* for 5 min and the pelleted cells were resuspended in DMEM + 10% FBS + 1% PS and plated. Upon confluence, the cells were differentiated according to the protocol as described previously (14, 15). Briefly, confluent cells in the stromal vascular fraction were plated in 1:1 surface ratio, and differentiation was induced 2 days afterwards by switching to a differentiation induction cocktail (DMEM containing 10% FBS, 1% PS, 0.5 mM isobutylmethylxanthine, 1 μM dexamethasone, 7 $\mu\text{g}/\text{ml}$ insulin, and 1 μM rosiglitazone) for 3 days. Subsequently, cells were maintained in DMEM supplemented

with 10% FBS, 1% PS, and 7 $\mu\text{g}/\text{ml}$ insulin for 3–6 days and switched to DMEM with 10% FBS and 1% PS for 3 days. The average rate of differentiation was at least 80% as determined by eye.

Cell culture experiments and chemical treatments

BMDMs and peritoneal macrophages were exposed to 0.5 mM intralipid or 0.5 mM oleic acid (Sigma-Aldrich) for 6 h in DMEM/PS media. The oleic acid was conjugated to BSA at a ratio of 2:1 (BSA:oleic acid). BMDMs were also treated with synthetic PPAR agonists (1 μM Wy14643, 1 μM rosiglitazone, 1 μM L165041, 1 μM GW501516) or vehicle control for 6 h. All PPAR agonists were obtained from Sigma-Aldrich. Peritoneal macrophages and RAW264.7 cells were incubated for 6 h with lymph (final triglyceride concentration of 2 mM, which was collected from rats provided with palm-oil based high fat diet overnight). BMDMs were co-incubated for 6 h with 10 μM orlistat (Sigma-Aldrich) and 0.5 mM intralipid. RAW264.7 macrophages treated with 0.5 mM intralipid or lymph were incubated with or without 0.5 $\mu\text{g}/\text{ml}$ recombinant ANGPTL4 (R&D Systems, Abingdon, UK). In a separate experiment, BMDMs of WT and *Angptl4*^{-/-} mice were exposed to the ER to Golgi transport inhibitors, monensin (10 μM , 3 h; Cayman Chemicals) and Brefeldin A (5 $\mu\text{g}/\text{ml}$, 4 h; Sigma-Aldrich), proteasomal degradation inhibitor, MG132 (40 μM , 4 h; Sigma-Aldrich), and lysosomal degradation inhibitors, e64d (20 μM , 24 h; Sigma-Aldrich) and leupeptin (5 μM , 16 h; Cayman Chemicals).

Oil Red O staining

Oil Red O staining was performed in RAW264.7 cells incubated with intralipid or lymph in the presence or absence of recombinant ANGPTL4. A stock of Oil Red O (Sigma) was prepared by dissolving 0.5 g in 500 ml of isopropanol. Working concentrations were made by dissolving stock concentrations with water (3 stock:2 water) and filtered. Treated cells were washed twice with PBS followed by fixation with 4% formalin for 30 min. The cells were then washed twice with PBS and incubated with Oil Red O dye for 20 min. The stained cells were washed three times with ddH₂O after which cells were visualized under a light microscope and pictures taken.

Bodipy staining

For visualization of lipid droplets, BMDMs of WT and *Angptl4*^{-/-} mice were washed with PBS, fixated in 4% formalin, and subsequently stained with 1 ng/ml Bodipy 493/503 (Thermo Fisher Scientific, Landsmeer, The Netherlands).

RNA isolation and quantitative real-time PCR

Total RNA was isolated from tissues and cells by homogenizing in TRIzol (Thermo Fisher Scientific) either with a QIAGEN Tissue Lyser II (QIAGEN, Venlo, The Netherlands) or by pipetting up and down. Reverse transcription was performed using the iScript™ cDNA synthesis kit (Bio-Rad) according to the manufacturer's protocol. Quantitative PCR amplifications were done on a CFX384 real-time PCR platform (Bio-Rad) with the SensiMix PCR mix from Bioline (GC Biotech, Alphen aan de Rijn, The Netherlands). Primer sequences of genes are provided in supplemental Table S1. Gene expression values were normalized to the housekeeping gene, *36b4* (*Rplp0*, ribosomal protein lateral stalk subunit P0).

Microarray analysis

RNeasy mini columns (QIAGEN) were used to isolate RNA from mouse peritoneal macrophages that were incubated for 6 h with 0.5 mM intralipid in the presence or absence of 2.5 $\mu\text{g}/\text{ml}$ recombinant ANGPTL4. RNA quality was verified on an Agilent 2100 bioanalyzer (Agilent Technologies, Amsterdam, The

Netherlands) using 6000 Nano chips according to the manufacturer's instructions. RNA was considered suitable for array hybridization only if the RNA integrity number exceeded 8.0. RNA from three samples per group was pooled for microarray analysis. One hundred nanograms of RNA were used for Whole Transcript cDNA synthesis (Affymetrix, Santa Clara, CA). Hybridization, washing, and scanning of Affymetrix GeneChip Mouse Gene 1.0 ST arrays were carried out according to standard Affymetrix protocols. Scans of the Affymetrix arrays were processed using packages from the Bioconductor project. Arrays were normalized using the Robust Multi-array Average method (37, 38). Probe sets were defined by assigning probes to unique gene identifiers, e.g., Entrez ID (39). Changes in gene expression were calculated as signal log ratios between treatment and control. These ratios were used to create heat maps within Excel. The CEL files were deposited in Gene Expression Omnibus (accession number GSE136240).

Affymetrix GeneChip analysis was carried out on WT mouse BMDMs incubated with oleate (250 μ M) for 5 h (40). CEL files were downloaded from the internet via Gene Expression Omnibus (GSE77104) and processed as described above.

Extracellular flux analysis

Real-time oxygen consumption rates (OCRs) of BMDMs from WT and *Angptl4*^{-/-} mice were assessed using XF-96 extracellular flux analyzer (Seahorse Bioscience, Santa Clara, CA). Basal metabolic rates of BMDMs seeded in quintuplicate were determined during three consecutive measurements in unbuffered Seahorse medium [8.3 g DMEM powder, 0.016 g phenol red, and 1.85 g NaCl in 1 liter milli-Q (pH 7.4) at 37°C, sterile-filtered] containing 25 mM glucose and 2 mM L-glutamine. Measurements were performed after 6 h treatment with intralipid (0.5 mM) in the presence or absence of recombinant ANGPTL4 (0.5 μ g/ml). After basal measurements, three consecutive measurements were made following addition of 1.5 μ M oligomycin, 1.5 μ M carbonyl cyanide 4-(trifluoromethoxy)phenylhydrazone (FCCP), and combination of 2 μ M antimycin A and 1 μ M rotenone. Pyruvate (1 mM) was added together with FCCP to fuel maximal respiration. All compounds used during the Seahorse runs were acquired from Merck. Signals were normalized to relative DNA content in the wells using the Quanti-iT™ dsDNA assay kit (Thermo Fisher Scientific).

Western immunoblotting

To isolate protein, mouse fat pads, differentiated primary adipocytes, primary macrophages, and whole adipose tissues were lysed in RIPA lysis and extraction buffer [25 mM Tris-HCl (pH 7.6), 150 mM NaCl, 1% Nonidet P-40, and 0.1% SDS; Thermo Fisher Scientific] supplemented with protease and phosphatase inhibitors (Roche Diagnostics, Almere, The Netherlands). Following homogenization, lysates were placed on ice for 30 min and centrifuged two or three times at 12,879 g for 10 min at 4°C to remove fat and cell debris. Concentration of protein lysates was determined using a bicinchoninic acid assay (Thermo Fisher Scientific). For assessment of LPL release, BMDMs were treated for 20 min with 10 IU/ml heparin (#012866-08; LEO Pharma). For assessment of glycosylation of LPL, 2–30 μ g of proteins were digested with endoglycosidase H (EndoH) (New England BioLabs) according to manufacturer's protocol. Protein lysates (10–30 μ g of protein per lane) were loaded onto 8–16% or 10% Criterion gels (Bio-Rad, Veenendaal, The Netherlands). Next, proteins were transferred onto a polyvinylidene difluoride membrane using the Transblot Turbo system (Bio-Rad). Membranes were probed with a goat anti-mouse LPL antibody (41), a rabbit anti-mouse HSP90 antibody (#4874S; Cell Signaling), a rat anti-mouse ANGPTL4 antibody (Kairos 142-2; Adipogen), and a rabbit anti-mouse

ANGPTL4 antibody (#742, home made) (42) at 1:5,000 (LPL), 1:2,000 (HSP90), or 1:1,000 (ANGPTL4) dilutions. Blocking and incubation of primary and secondary antibodies were done in TBS (pH 7.5) plus 0.1% Tween 20 (TBS-T) and 5% (w/v) skimmed milk at 1:5,000. In between, membranes were washed in TBS-T. Quantification was performed with the ChemiDoc MP system (Bio-Rad) and Clarity ECL substrate (Bio-Rad). Equal loading of medium samples was verified with HSP90.

Statistical analysis

Statistical analyses were performed using one-way ANOVA followed by Tukey HSD test or by Student's *t*-test. Data are presented as mean \pm SEM (animal experiments) or mean \pm SD (cell culture studies). *P* < 0.05 was considered statistically significant.

RESULTS

Angptl4 expression is sensitive to lipids and regulates lipid uptake in macrophages

We previously suggested that enhanced LPL-mediated lipid uptake in macrophages may be at the basis of the mesenteric lymphadenopathy in *Angptl4*^{-/-} mice fed a high fat diet (29). To better understand the role of endogenous ANGPTL4 in lipid uptake in macrophages, we first studied the regulation of *Angptl4* expression by lipids in macrophages. Treatment of peritoneal macrophages with oleic acid markedly increased *Angptl4* mRNA (Fig. 1A). Similarly, treatment of peritoneal macrophages and BMDMs with intralipid markedly induced *Angptl4* mRNA (Fig. 1B). Interestingly, analysis of a publicly available transcriptomics dataset indicated that *Angptl4* is the most highly induced gene in BMDMs upon treatment with oleic acid (Fig. 1C) (40). Treatment of BMDMs with the synthetic PPAR γ agonist, rosiglitazone, and the synthetic PPAR δ agonists, L165041 and GW501516, markedly increased *Angptl4* mRNA (Fig. 1D). By contrast, the PPAR α agonist, Wyl4643, had no effect on *Angptl4* expression. These data suggest that the effect of lipid treatment on *Angptl4* expression in BMDMs might be mediated by PPAR δ and/or PPAR γ .

To study the effect of exogenous ANGPTL4 on lipid uptake in macrophages, RAW264.7 macrophages were treated with intralipid in the presence or absence of recombinant ANGPTL4. ANGPTL4 clearly reduced lipid accumulation, as shown by decreased Oil Red O staining (Fig. 2A). Similar results were obtained in peritoneal macrophages incubated with lymph, an endogenous lipid source (Fig. 2B). Transcriptomics analysis of peritoneal macrophages treated with intralipid showed that the induction of lipid-sensitive genes by intralipid was almost completely abolished in the presence of recombinant ANGPTL4 (Fig. 2C).

To study the effect of endogenous ANGPTL4 on lipid uptake in macrophages, WT and *Angptl4*^{-/-} BMDMs were treated with intralipid. Lipid accumulation was distinctly higher in *Angptl4*^{-/-} macrophages than in WT macrophages, as shown by Bodipy staining (Fig. 2D). This effect could be abolished by treatment with orlistat, a general serine hydrolase inhibitor that targets LPL (Fig. 2D). Consistent with enhanced lipid uptake in *Angptl4*^{-/-} macrophages,

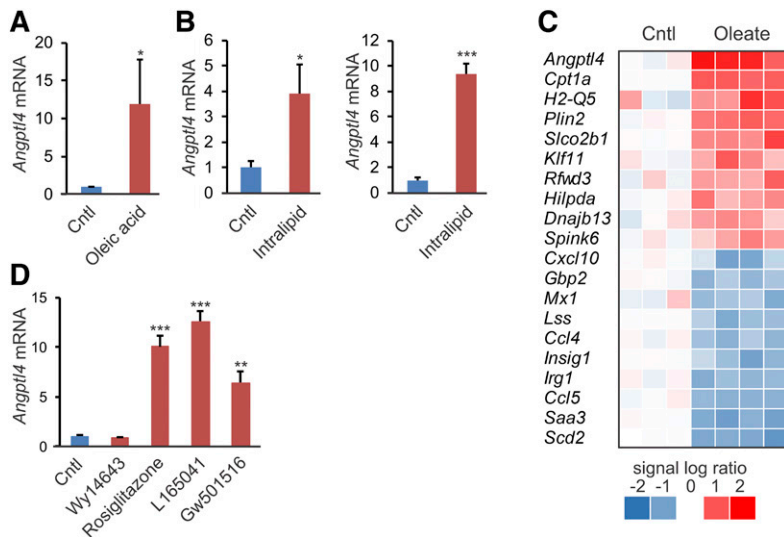


Fig. 1. *Angptl4* expression is induced in primary macrophages by lipid stimulation or PPAR agonists. **A:** *Angptl4* expression in peritoneal macrophages treated with 0.5 mM oleic acid for 6 h. **B:** *Angptl4* expression in peritoneal macrophages (left) and BMDMs (right) treated for 6 h with 0.5 mM intralipid. **C:** Heat map of top 10 most upregulated and top 10 most downregulated genes in BMDMs treated for 5 h with 250 uM oleic acid or BSA (vehicle control). Data are from a previously published dataset (GSE77104) (43). **D:** *Angptl4* expression in BMDMs treated for 6 h with 1 μ M of PPAR agonists, Wy14643 (PPAR α), GW501516 (PPAR δ), L165041 (PPAR δ), and rosiglitazone (PPAR γ), or vehicle (DMSO). mRNA expression was normalized to *36b4*. Data are mean \pm SD from three biological replicates; * $P < 0.05$, ** $P < 0.01$, and *** $P < 0.001$ relative to vehicle control.

the effect of intralipid on the expression of lipid-sensitive genes was much more pronounced in *Angptl4*^{-/-} BMDMs than in WT BMDMs (Fig. 2E). Similar results were obtained in peritoneal WT and *Angptl4*^{-/-} macrophages upon loading with lymph (Fig. 2F). Together, these data strongly suggest that ANGPTL4 controls lipid uptake in macrophages via regulation of LPL.

ANGPTL4 deficiency increases respiration in BMDMs but does not influence LPL levels

To determine whether differences in lipid uptake between the genotypes are reflected in fuel utilization, we measured real-time metabolic fluxes in BMDMs using the Seahorse machine (Fig. 3A). Interestingly, after intralipid treatment, basal and maximal respiration was significantly higher in *Angptl4*^{-/-} than in WT macrophages (Fig. 3B). Treatment with exogenous ANGPTL4, despite leading to slightly lower values, did not significantly influence basal and maximal respiration in *Angptl4*^{-/-} BMDMs. These data suggest that the inhibitory effect of endogenous ANGPTL4 on LPL-mediated lipid uptake in macrophages is accompanied by a decrease in fuel utilization.

We previously showed in primary adipocytes that ANGPTL4 deficiency is paralleled by elevated LPL protein levels (26). To study the influence of ANGPTL4 deficiency on LPL protein in macrophages, we performed Western blot for LPL in BMDMs from WT and *Angptl4*^{-/-} mice, with and without intralipid treatment. In contrast to what was observed in adipocytes, ANGPTL4 deficiency did not have any effect on LPL protein in macrophages and did not alter the ratio between the active endonuclease H-resistant form and the inactive endonuclease-sensitive form of LPL (Fig. 3C). In addition, the amount of LPL that could be released into the medium by treatment of the macrophages with heparin did not differ between the two genotypes (Fig. 3D).

Additional experiments showed that inhibition of ER to Golgi transport by monensin and Brefeldin A increased intracellular LPL levels, as did inhibition of proteasomal degradation by MG132, albeit to a lesser extent (Fig. 3E). By contrast, inhibition of lysosomal proteases using leupeptin and e64d did not alter intracellular LPL accumulation in

BMDMs (Fig. 3E). These data suggest that unlike LPL in adipocytes, LPL in macrophages is not subject to lysosomal degradation but instead is broken down, at least partly, via proteasomal degradation. Interestingly, none of these effects were influenced by ANGPTL4 deficiency (Fig. 3E). These data indicate that in macrophages, inhibition of LPL activity by ANGPTL4 is not accompanied by a decrease in LPL protein levels.

Angptl4-hypomorphic mice show partial expression of N-terminal exons and truncated ANGPTL4 protein in adipocytes

The second objective of this work was to investigate whether, in addition to the *Angptl4*^{-/-} model, an alternative model of genetic *Angptl4* inactivation also leads to a deleterious phenotype in mice fed a high saturated fat diet. To that end, we used *Angptl4* knockout first mice. The *Angptl4* knockout first allele contains in intron 3 a reading frame-independent LacZ gene trap cassette followed by a promoter-driven selection cassette (Fig. 4A). The *Angptl4* knockout first allele was designed to create tissue-specific *Angptl4*^{-/-} mice by subsequent crossing with mice expressing the FLP and Cre recombinase enzymes. Interestingly, based on sequence analysis, it can be predicted that when omitting the FLP and Cre recombinase reaction steps, the *Angptl4* knockout first allele might lead to the production of a whole-body mutant 32 kDa ANGPTL4 protein covering amino acid residues 1–186, followed by 102 amino acids originating from the EN2a splice acceptor site and the internal ribosome entry site (Fig. 4B). Accordingly, we hypothesized that the *Angptl4* knockout first allele may give rise to a truncated ANGPTL4 protein that contains the N-terminal domain responsible for LPL inhibition. Below, we will refer to the ANGPTL4 knockout first mice as *Angptl4*^{hyp} mice, as explained below.

To carefully characterize the *Angptl4*^{hyp} mice, we performed quantitative (q)PCR for *Angptl4* using cDNA obtained from adipose tissue and primary adipocytes of WT, *Angptl4*^{hyp}, and *Angptl4*^{-/-} mice. Primers were designed to amplify parts of the cDNA encoded by specific exons. Remarkably, whereas no *Angptl4* expression using any of

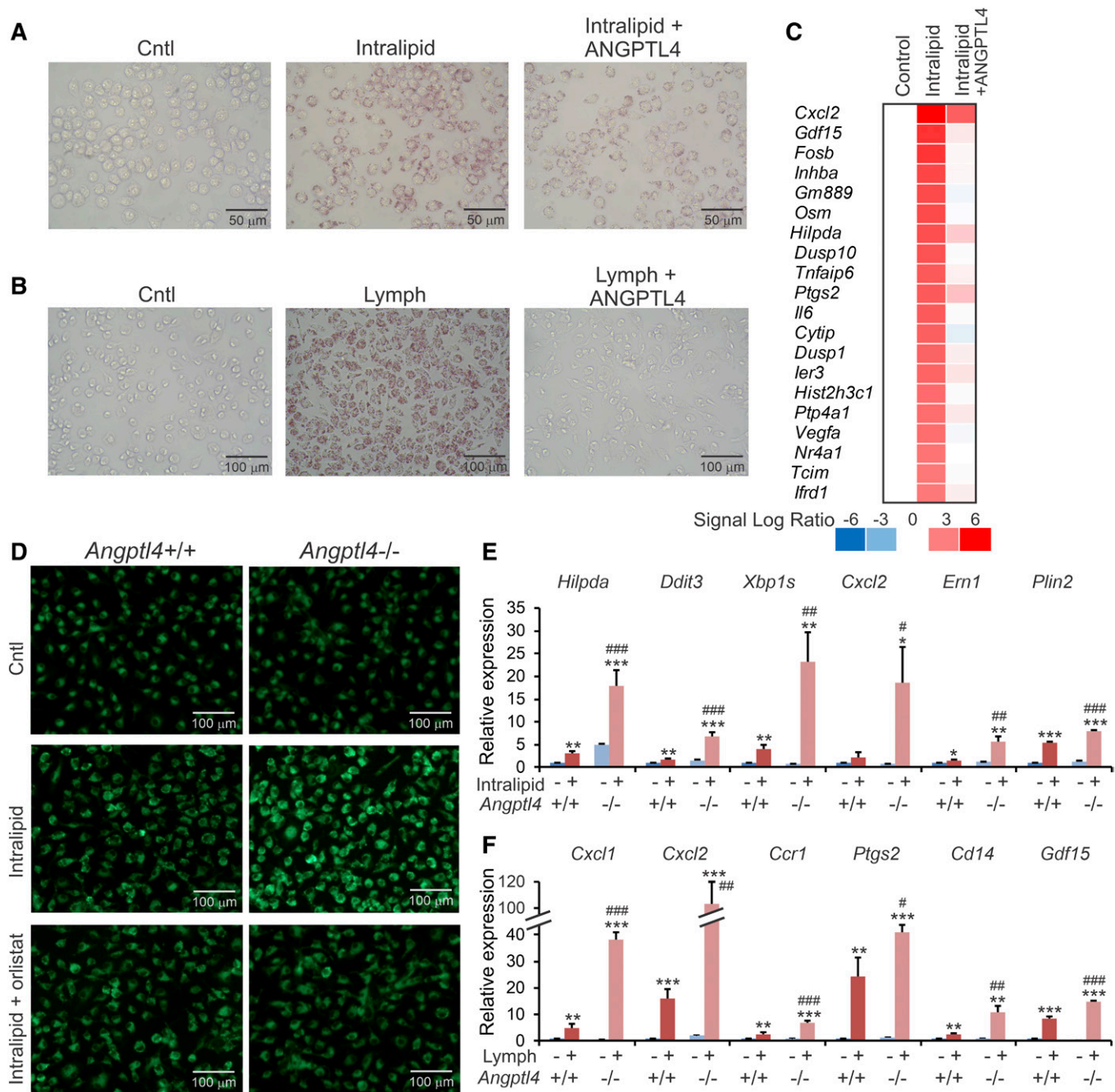


Fig. 2. ANGPTL4 deficiency promotes macrophage lipid uptake and magnifies the induction of lipid-sensitive genes. **A:** Oil Red O staining of lipid droplets in RAW264.7 macrophages treated with 0.5 mM intralipid for 6 h in the presence or absence of 0.5 μ g/ml recombinant ANGPTL4. **B:** Oil Red O staining of lipid droplets in peritoneal macrophages treated for 6 h with lymph (final triglyceride concentration of 2 mM) in the presence or absence of 0.5 μ g/ml recombinant ANGPTL4. **C:** Microarray heat map showing expression profile of lipid-sensitive genes in peritoneal macrophages treated for 6 h with 0.5 mM intralipid in the presence or absence of recombinant ANGPTL4. **D:** Bodipy staining of *Angptl4*^{+/+} and *Angptl4*^{-/-} BMDMs cultured with regular culture medium (Cntl) or for 6 h with 0.5 mM intralipid with or without orlistat. **E, F:** mRNA expression of lipid-sensitive genes in *Angptl4*^{+/+} and *Angptl4*^{-/-} BMDMs treated for 6 h with 0.5 mM intralipid (**E**) or peritoneal macrophages treated for 6 h with lymph (final triglyceride concentration of 2 mM) (**F**). mRNA expression was normalized to *36b4*. Data are mean \pm SD from three biological replicates; * P < 0.05, ** P < 0.01, and *** P < 0.001 relative to untreated WT; and # P < 0.05, ## P < 0.01, and ### P < 0.001 relative to WT + intralipid/lymph.

the primers could be detected in adipose tissue and adipocytes of *Angptl4*^{-/-} mice, substantial *Angptl4* expression (approximately 30–50% of WT level) for exons 1–3 was found in the *Angptl4*^{hyp} mice (Fig. 4C, D). By contrast, no amplification was observed in the *Angptl4*^{hyp} mice using primers directed against the cDNA encoded by exons 4–7

(Fig. 4C, D). A similar expression profile of the *Angptl4* exons was observed in the liver of *Angptl4*^{hyp} mice (supplemental Fig. S1A). Further PCR analysis of the cDNA suggested the presence of a mRNA comprising *Angptl4* exons 1–3, the EN2a splice acceptor site, and more than 50% of the IRES site, but without the LacZ gene (supplemental

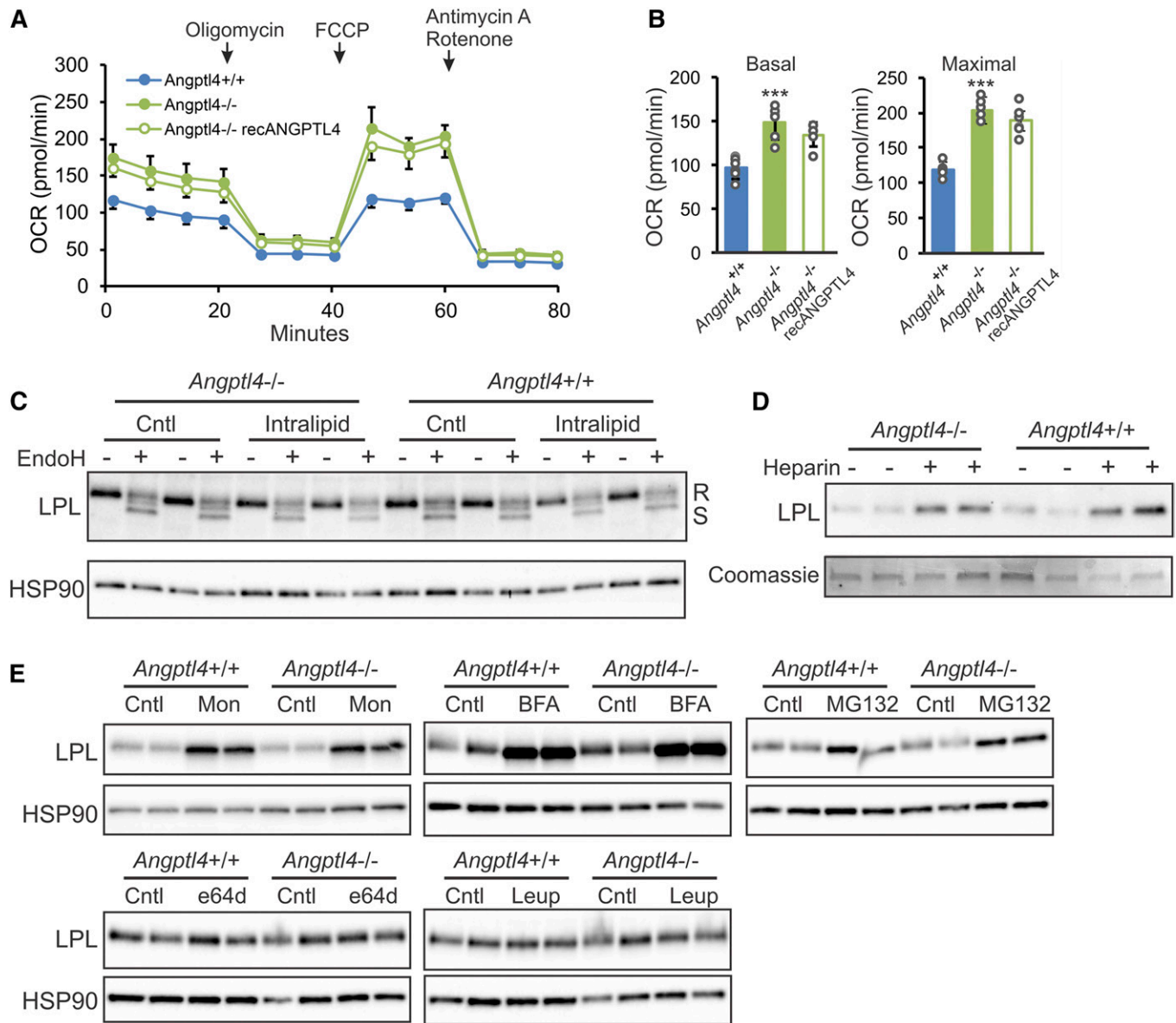


Fig. 3. ANGPTL4 deficiency increases respiration in BMDMs but does not influence LPL abundance. A: Real-time changes in OCR in BMDMs from *Angptl4*^{+/+} and *Angptl4*^{-/-} mice in the presence or absence of recombinant ANGPTL4, treated with 0.5 mM intralipid for 6 h, and assessed in unbuffered medium during sequential injections with oligomycin, FCCP, and antimycin A + rotenone. B: Basal (left) and maximal (right) OCR in BMDMs from *Angptl4*^{+/+} and *Angptl4*^{-/-} mice in the presence or absence of recombinant ANGPTL4 (0.5 μg/ml) incubated with 0.5 mM intralipid for 6 h. Measurements were done in quintuplicates in unbuffered medium. Data are mean ± SD; ****P* < 0.001. C: Immunoblot of LPL in *Angptl4*^{+/+} and *Angptl4*^{-/-} BMDMs treated for 6 h with or without 0.5 mM intralipid in the presence or absence of endonuclease-H. D: Immunoblot of LPL from culture medium of *Angptl4*^{+/+} and *Angptl4*^{-/-} BMDMs treated with or without heparin. E: Immunoblot of LPL in *Angptl4*^{+/+} and *Angptl4*^{-/-} BMDMs treated with or without ER to Golgi transport inhibitors monensin (Mon; 10 μM for 3 h) and Brefeldin A (BFA; 5 μg/ml for 4 h), proteasomal degradation inhibitor MG132 (40 μM for 4 h), and lysosomal degradation inhibitors, e64d (20 μM for 24 h) and leupeptin (Leup; 5 μM for 16 h). HSP90 or Coomassie staining serve as loading control.

Table S2). These data indicate that the *Angptl4*^{hyp} mice produce a mutated cDNA that may lead to the production of a truncated ANGPTL4 protein.

To verify this notion, we performed Western blot on adipose tissue of the three types of mice using a monoclonal antibody directed against mouse ANGPTL4. A strong ANGPTL4 band at 50 kDa was observed in the WT mice (Fig. 4E). At this position, a weak band was observed in the *Angptl4*^{hyp} and *Angptl4*^{-/-} mice, which is likely nonspecific. Interestingly, a band of around 32 kDa corresponding to

the predicted size for the truncated ANGPTL4 protein was observed in the *Angptl4*^{hyp} mice but not in the *Angptl4*^{-/-} mice (Fig. 4E). To verify that the designated bands indeed represent ANGPTL4, we used the same samples to perform Western blot using a polyclonal antibody directed against an epitope close to the N terminus of ANGPTL4. Similar results were obtained (Fig. 4E). These analyses confirm that the *Angptl4*^{hyp} mice produce a truncated ANGPTL4 protein containing the LPL inhibitory domain at levels that are far below the levels in WT mice. Accordingly,

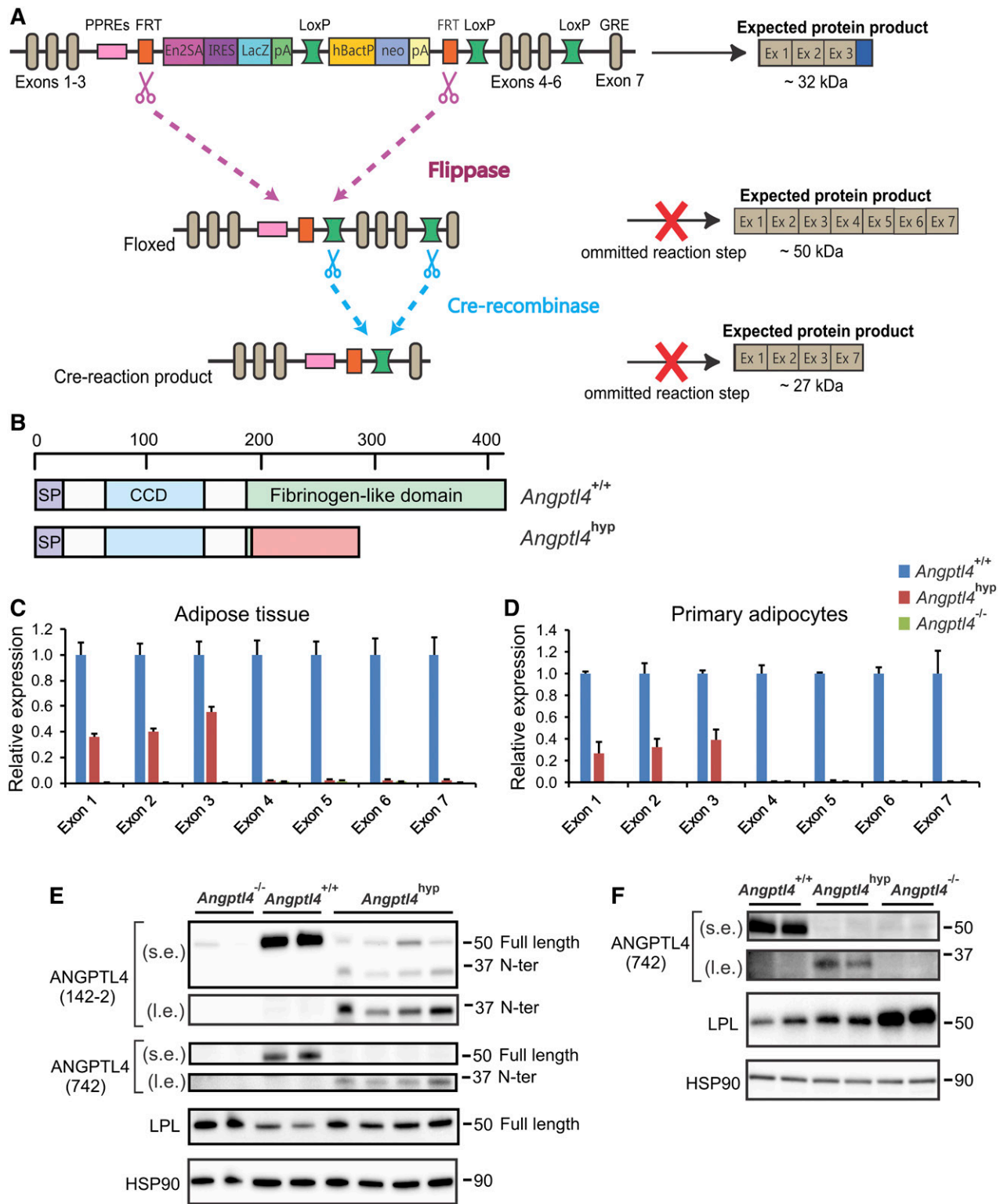


Fig. 4. Hypomorphic ANGPTL4 mice show reduced ANGPTL4 expression and reduced regulation on LPL. **A:** Schematic map of the *Angptl4* locus by knockout first-allele strategy. **B:** Full ANGPTL4 protein (upper scheme) and predicted sequence of truncated ANGPTL4 (lower scheme) based on sequence analysis of the knockout first-allele mice. mRNA expression of all seven exons of *Angptl4* in epididymal adipose tissue (**C**) and primary adipocytes (**D**) of *Angptl4*^{-/-} and *Angptl4*^{hyp} mice relative to WT mice. Western blot showing full-length and N-terminal ANGPTL4, and LPL in adipose tissue (**E**) and primary adipocytes (**F**) of the *Angptl4*^{-/-}, *Angptl4*^{hyp}, and WT mice. mRNA expression was normalized to *36b4*. Data are mean \pm SEM. N = 7–11 mice per group. s.e., short exposure; l.e., long exposure.

the *Angptl4*^{hyp} mice represent a hypomorph. In line with previous studies, LPL protein levels were increased in adipose tissue of *Angptl4*^{-/-} mice (Fig. 4E) (26, 27). LPL

protein levels were also increased in *Angptl4*^{hyp} mice compared with WT mice (Fig. 4E, supplemental Fig. S1B). Similarly, primary adipocytes of *Angptl4*^{hyp} mice expressed

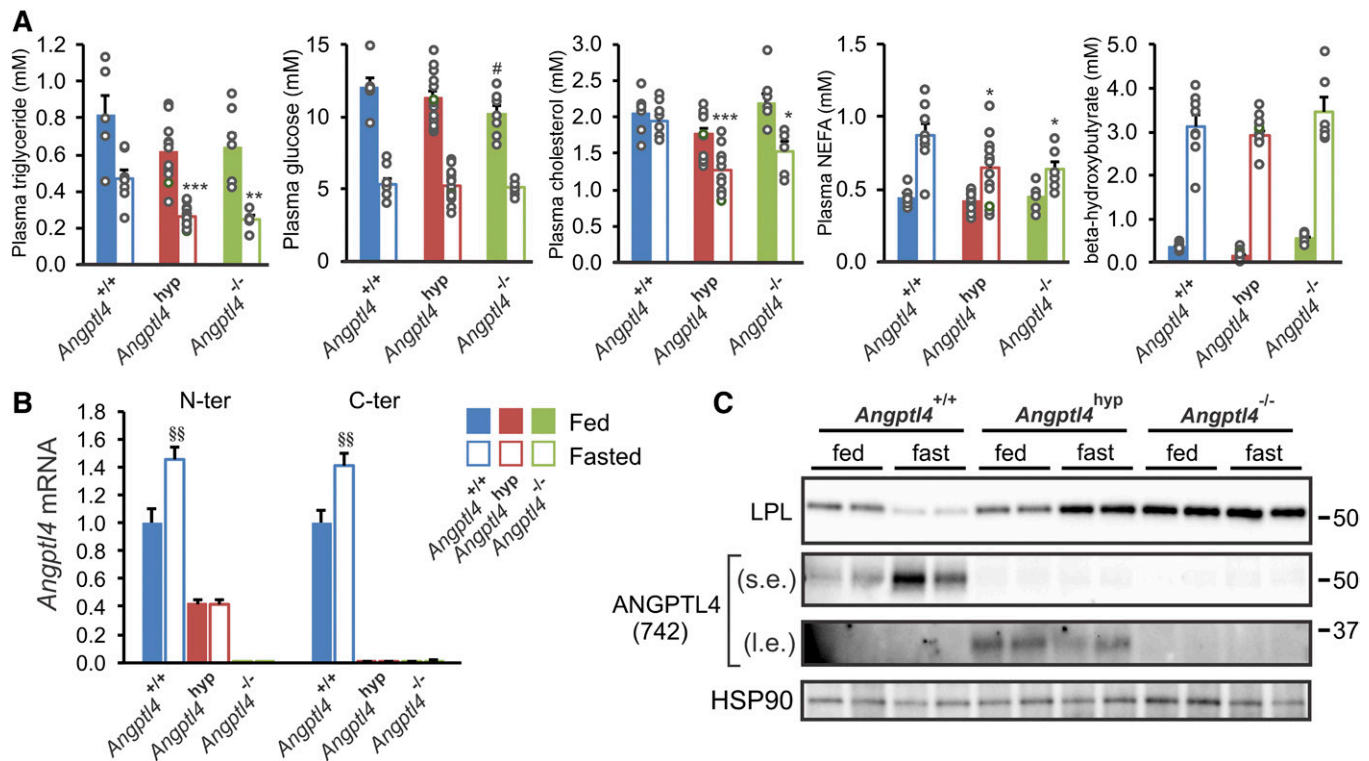


Fig. 5. Similar regulation on plasma metabolites and LPL between *Angptl4*^{hyp} and *Angptl4*^{-/-} mice after 24 h fast. **A:** Plasma levels of triglycerides, glucose, cholesterol, NEFAs, and β -hydroxybutyrate in fed (closed bars) and fasted (opened bars) mice. **B:** mRNA expression from N-terminal (left column) and C-terminal (right column) regions of *Angptl4* in epididymal adipose tissues of fed (closed bars) and fasted (opened) mice. **C:** Western blot of LPL and ANGPTL4 in epididymal adipose tissues from the three groups of mice in fed and fasted state. mRNA expression was normalized to *36b4*. Data are mean \pm SEM. N = 7–11 mice per group. * P < 0.05, ** P < 0.01, and *** P < 0.001 represent significance in fasted group relative to WT fasted mice; # P < 0.05 represents significance in fed group relative to WT fed mice; and §§ P < 0.01 relative to WT fed mice. s.e., short exposure; l.e., long exposure.

low levels of a truncated N-terminal ANGPTL4 protein (Fig. 4F, supplemental Fig. S1C). Consistent with an effect of truncated ANGPTL4 on LPL abundance, LPL protein levels in *Angptl4*^{hyp} adipocytes were markedly lower than in *Angptl4*^{-/-} adipocytes, yet higher than in WT adipocytes (Fig. 4F).

Angptl4^{hyp} and *Angptl4*^{-/-} mice have similar plasma triglycerides and adipose LPL protein levels after a 24 h fast

In line with the alternative name, fasting-induced adipose factor, the effects of *Angptl4* inactivation or overexpression on lipid metabolism are most prominent in the fasted state. Accordingly, we measured basic plasma parameters in the three types of mice in the fasted and fed state. Fasting plasma levels of triglycerides, cholesterol, and NEFAs were very similar between the *Angptl4*^{hyp} and *Angptl4*^{-/-} mice, and were significantly lower compared with the WT mice (Fig. 5A). These data suggest that *Angptl4*^{hyp} and *Angptl4*^{-/-} mice are highly similar and that the low levels of N-terminal ANGPTL4 protein in the *Angptl4*^{hyp} mice have no discernible impact on plasma lipid parameters in the fasted state.

Consistent with previous studies (11, 35), *Angptl4* mRNA in adipose tissue was significantly increased by fasting (Fig. 5B). Interestingly, fasting did not influence *Angptl4* mRNA in the *Angptl4*^{hyp} mice. In line with these

data and fitting with previous studies (27, 43), ANGPTL4 protein levels in WT adipose tissue were increased by fasting, concomitant with a decrease in LPL protein levels (Fig. 5C, supplemental Fig. S1D). By contrast, levels of truncated ANGPTL4 protein remained unchanged or tended to decrease during fasting in the *Angptl4*^{hyp} mice, while LPL protein levels went up (Fig. 5C, supplemental Fig. S1D, E).

As previously shown (27), LPL protein was higher in *Angptl4*^{-/-} mice compared with WT mice (Fig. 5C). Importantly, the decrease in LPL protein upon fasting was abrogated in *Angptl4*^{-/-} mice, indicating that the increase in ANGPTL4 mediates the reduction in LPL protein upon fasting. Interestingly, in the fed state, LPL protein levels were lower in *Angptl4*^{hyp} than *Angptl4*^{-/-} mice, whereas in the fasted state, LPL protein levels were similar in *Angptl4*^{hyp} and *Angptl4*^{-/-} mice (Fig. 5C, supplemental Fig. S1D). These data suggest that small amounts of N-terminal ANGPTL4 in adipose tissue can decrease LPL protein levels, presumably by promoting LPL degradation, specifically in the fed and not the fasted state.

Angptl4^{hyp} mice show attenuated chylous ascites and acute inflammation but similar levels of lymphadenopathy as *Angptl4*^{-/-} mice

We have previously shown that *Angptl4*^{-/-} mice respond poorly to a high-saturated fat diet showing the formation of

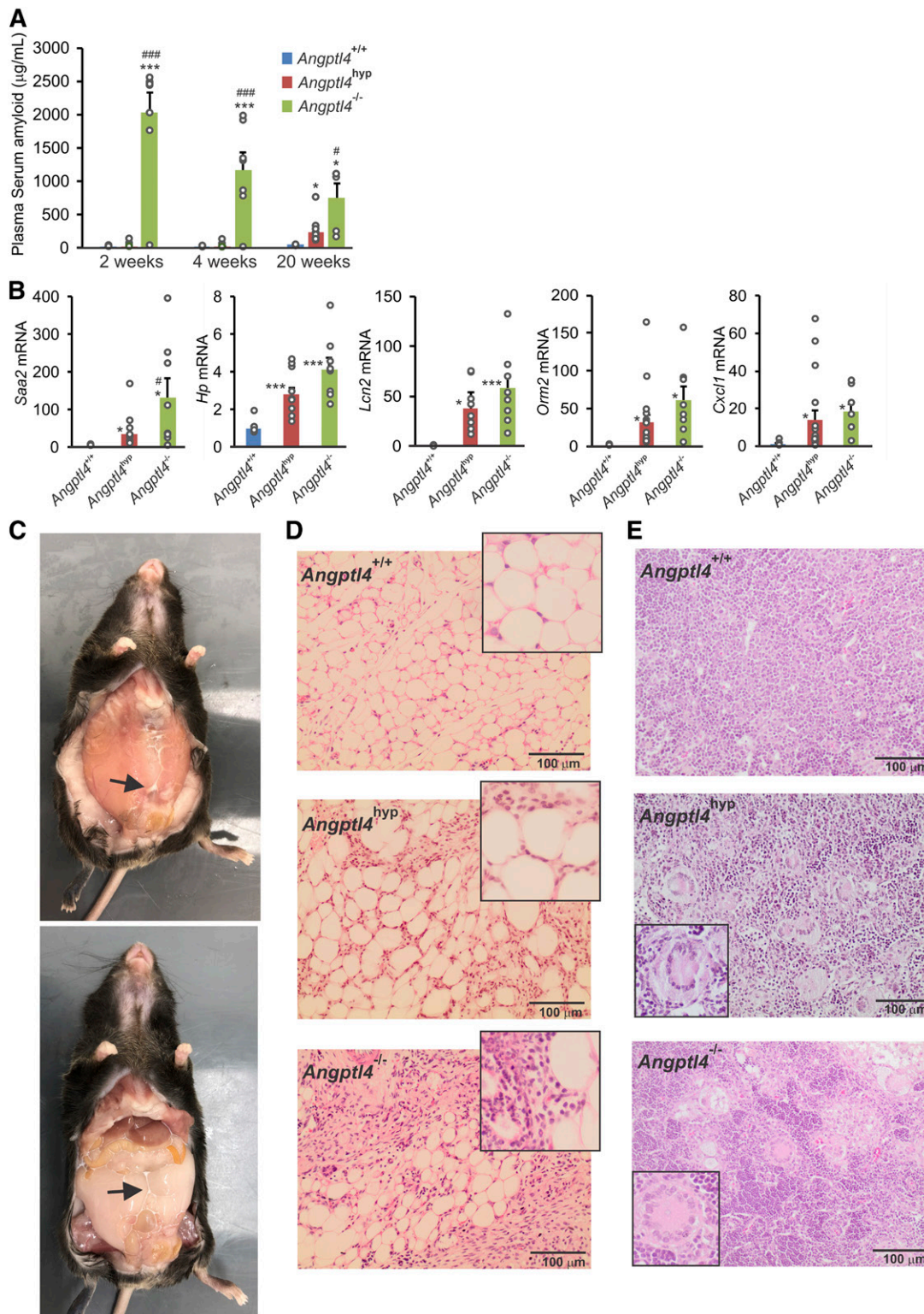


Fig. 6. *Angptl4^{hyp}* mice have less severe pathological phenotypes in response to 20 weeks of high fat diet compared with *Angptl4^{-/-}* mice. A: Plasma levels of SAA after 2, 4, and 20 weeks of high fat diet. B: Relative hepatic expression of pro-inflammatory markers in three groups of mice. C: Pictures showing levels of ascites formation in the peritoneum of *Angptl4^{hyp}* mice. Arrows pointing toward ascites. D: H&E staining depicting mesenteric panniculitis in *Angptl4^{hyp}* mice. E: Images showing Touton giant cells in the mesenteric lymph nodes of *Angptl4^{hyp}* and *Angptl4^{-/-}* mice but not WT mice. Images are 200× magnification; insert is 400× magnification. mRNA expression was normalized to *36b4*. Data are mean ± SEM. N = 7–11 mice per group. **P* < 0.05, ***P* < 0.01, and ****P* < 0.001 relative to WT.

lipid-laden Touton giant cells in mesenteric lymph nodes, chylous ascites, and acute inflammation (30). To determine the influence of low levels of N-terminal ANGPTL4

on the development of mesenteric lymphadenopathy, chylous ascites, and other pathologies, the three groups of mice were fed a standard high fat diet rich in saturated fat

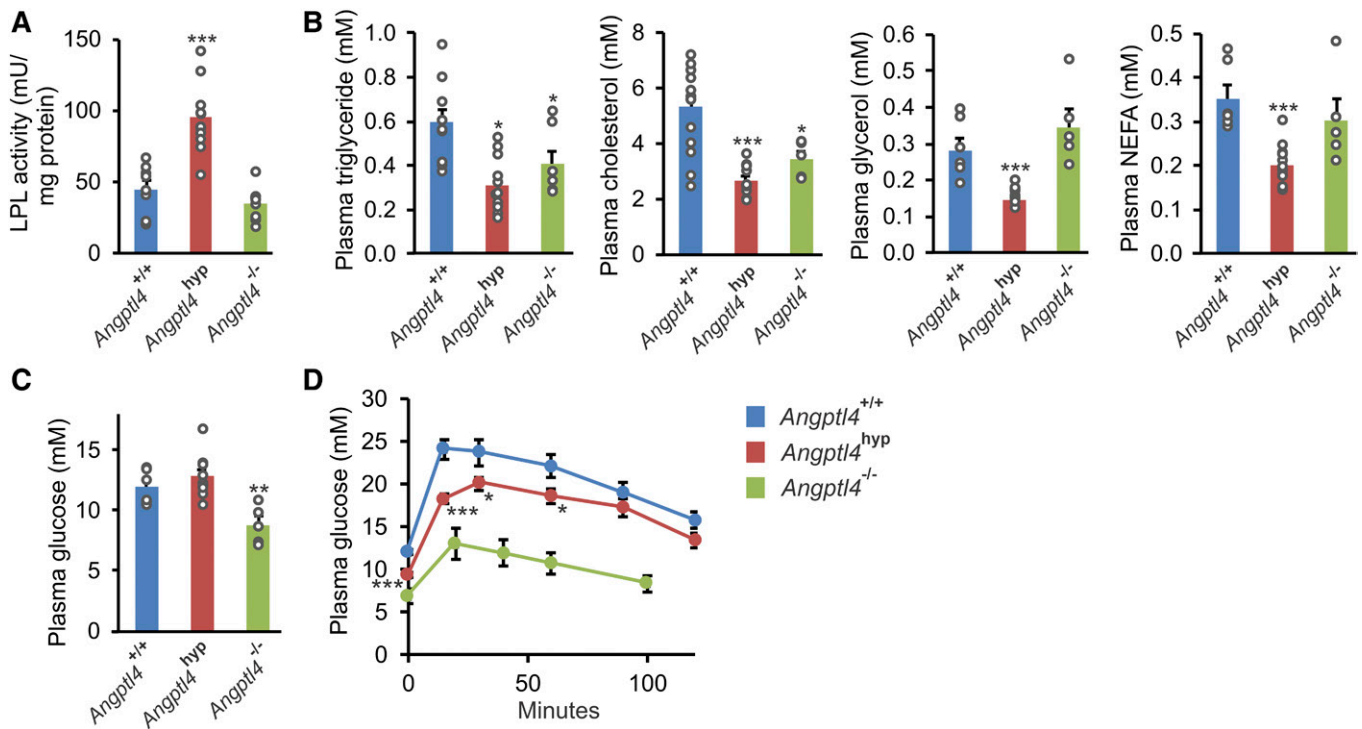


Fig. 7. Increased LPL activity and improved glucose tolerance in *Angptl4^{hyp}* mice after 20 weeks of high fat diet. A: LPL activity in epididymal adipose tissue of *Angptl4^{hyp}*, *Angptl4^{-/-}*, and WT mice. B: Plasma concentrations of triglycerides, cholesterol, glycerol, and NEFAs in the three groups of mice. Plasma glucose levels (C) and glucose tolerance test (D) in the three groups of mice. Data are mean \pm SEM. N = 7–11 mice per group. * $P < 0.05$, ** $P < 0.01$, and *** $P < 0.001$ relative to WT. No statistical analysis could be done on glucose tolerance in *Angptl4^{-/-}* mice due to the use of different time points.

for 20 weeks. Whereas the *Angptl4^{-/-}* mice showed a rapid and marked increase in SAA levels upon high fat feeding, SAA levels in the *Angptl4^{hyp}* mice only went up after 20 weeks of high fat feeding (Fig. 6A). At this time point, hepatic expression of several acute-phase proteins in *Angptl4^{hyp}* mice was significantly lower than or approximating the levels in *Angptl4^{-/-}* mice (Fig. 6B). Besides a delayed increase in SAA, the development of chylous ascites was much reduced in the *Angptl4^{hyp}* mice compared with the *Angptl4^{-/-}* mice. Whereas seven out of eight *Angptl4^{-/-}* mice showed very pronounced ascites several weeks after starting the high fat diet, leading to premature death in 6 *Angptl4^{-/-}* mice (30), at the end of the 20 weeks of high fat feeding, all *Angptl4^{hyp}* mice survived, with only two out of eleven *Angptl4^{hyp}* mice showing ascites, which was also very mild (Fig. 6C) (29, 30). The mesenteric adipose tissue of the *Angptl4^{hyp}* mice with ascites showed the characteristic mesenteric panniculitis, but this was less severe than in the *Angptl4^{-/-}* mice (Fig. 6D). Of note, the frequency rate, severity of ascites, and full survival in the *Angptl4^{hyp}* mice remained unchanged when extending the high fat feeding to 36 weeks in seven *Angptl4^{hyp}* mice (data not shown). Despite the much milder ascites and slower progression of the inflammatory phenotype, after 20 weeks of high fat feeding, nearly all mesenteric lymph nodes in the *Angptl4^{hyp}* mice contained multiple lipid-laden Touton giant cells (Fig. 6E). Specifically, Touton giant cells were present in the mesenteric lymph nodes of 10 out of 11 *Angptl4^{hyp}* mice and 7 out of 8 *Angptl4^{-/-}* mice but in none of the WT mice.

A summary of the clinical outcomes in the three groups of mice is presented in supplemental Table S3.

Angptl4^{hyp} mice show increased LPL activity and improved glucose tolerance compared with WT mice

Consistent with the role of ANGPTL4 as LPL inhibitor, after 20 weeks of high fat feeding, adipose tissue LPL activity was significantly higher in *Angptl4^{hyp}* mice than in WT mice (Fig. 7A). By contrast, adipose tissue LPL activity was not increased in *Angptl4^{-/-}* mice, which is likely related to the steatitis in these animals (29). Interestingly, whereas plasma levels of triglycerides and cholesterol were significantly lower in both *Angptl4^{hyp}* and *Angptl4^{-/-}* mice than in WT mice, plasma glycerol and NEFAs were only lower in the *Angptl4^{hyp}* mice, which again may be related to the steatitic phenotype of the *Angptl4^{-/-}* adipose tissue (Fig. 7B). To study the impact of ANGPTL4 deficiency on glucose homeostasis, we measured plasma glucose and performed a glucose tolerance test. Plasma glucose levels were significantly lower in *Angptl4^{-/-}* mice than in WT and *Angptl4^{hyp}* mice (Fig. 7C), while glucose tolerance was dramatically or modestly improved in *Angptl4^{-/-}* and *Angptl4^{hyp}* mice, respectively, compared with WT mice (Fig. 7D). Overall, the LPL activity and plasma metabolite levels in *Angptl4^{hyp}* mice are consistent with the known role of ANGPTL4 in intra- and extracellular lipolysis (44). By contrast, LPL activity and plasma metabolite levels in *Angptl4^{-/-}* mice fed a high fat diet likely partly reflect the severe inflammatory phenotype in these animals (29, 30).

DISCUSSION

In this work, we addressed two independent questions relevant to the mesenteric lymphadenopathy phenotype in *Angptl4*^{-/-} mice fed a high fat diet: 1) what is the influence of endogenous ANGPTL4 on lipid uptake and utilization in macrophages; and 2) what is the role of N-terminal ANGPTL4 in the development of mesenteric lymphadenopathy, inflammation, and ascites?

Our study confirms previous data indicating that *Angptl4* expression in macrophages is highly induced by lipids (29, 45, 46). This induction is likely mediated by PPAR δ and/or PPAR γ , as shown by the marked upregulation of *Angptl4* mRNA by PPAR δ and PPAR γ agonists in BMDMs. Importantly, the present study shows that not only external ANGPTL4 but also endogenously produced ANGPTL4 inhibits lipid uptake in macrophages. The elevated lipid uptake in *Angptl4*^{-/-} macrophages increases the expression of various lipid-sensitive genes involved in inflammation and ER stress, such as *Hilpda*, *Ddit3*, *Ptgs2*, and *Cxcl2*. Interestingly, the elevated lipid uptake in *Angptl4*^{-/-} macrophages was accompanied by increased mitochondrial respiration, suggesting that enhanced lipid uptake may stimulate cellular respiration. As the effect on cellular respiration was observed for endogenous and not exogenous ANGPTL4, it might reflect an intracellular mechanism of action of ANGPTL4. Together, our findings demonstrate an important role of ANGPTL4 in regulating lipid uptake and utilization in macrophages.

It is well-established that ANGPTL4 inactivates LPL by promoting LPL unfolding (24, 25). Recently, we found that ANGPTL4 has a local role in adipocytes by promoting the intracellular cleavage and subsequent degradation of LPL (26, 27). In stark contrast to adipocytes, ANGPTL4 deficiency in macrophages did not lead to the accumulation of full-length rapidly releasable LPL, while the cleaved N-terminal LPL portion was not detectable in our hands. The lack of effect of ANGPTL4 on LPL protein levels in macrophages may be because macrophage LPL is not degraded via the lysosomal pathway but via the proteasomal pathway. The difference in the LPL degradation pathway and in the effect of ANGPTL4 on LPL levels between adipocytes and macrophages could be connected to how LPL is presented on the cell surface. Specifically, it is conceivable that LPL on the surface of macrophages is not internalized for degradation, unlike LPL in adipocytes, and that ANGPTL4 only causes the unfolding and inactivation of LPL after both proteins have been secreted (47, 48). Overall, these findings suggest that the location and cellular mechanism of LPL inactivation by ANGPTL4 may be different in different cells.

Previously, we showed that *Angptl4*^{-/-} mice fed a diet rich in saturated fat develop an inflammatory and ultimately lethal phenotype characterized by the formation of Touton giant cells in mesenteric lymph nodes, chylous ascites, and fibrinopurulent peritonitis (29, 30). By comparing *Angptl4*^{-/-} mice with an *Angptl4*-hypomorphic model, here we show that a low-level expression of a truncated N-terminal ANGPTL4 does not prevent Touton giant cell formation, yet drastically mitigates the acute-phase response and the

development of chylous ascites upon high fat feeding. Importantly, the development of fibrinopurulent peritonitis and the death of the animals is completely prevented by the expression of the truncated N-terminal ANGPTL4. Although the severity of the clinical phenotype was attenuated, activation of the acute-phase response and chylous ascites were still observed in a substantial number of *Angptl4*^{hyp} mice.

Strictly, we cannot fully exclude that N-terminal ANGPTL4 influences ascites independently of LPL inhibition. However, two lines of reasoning support an action of N-terminal ANGPTL4 on ascites via LPL. First, LPL protein levels in *Angptl4*^{hyp} adipocytes were lower than in *Angptl4*^{-/-} adipocytes, paralleled by a marked reduction in ascites severity. These data suggest that a low level of N-terminal ANGPTL4 decreases LPL abundance. Second, chronic injection of a monoclonal antibody that is directed against N-terminal ANGPTL4 and abolishes its ability to inhibit LPL causes ascites in mice fed a HFD (28). Collectively, we favor the notion that the attenuation of the ascites phenotype in *Angptl4*^{hyp} mice compared with *Angptl4*^{-/-} mice is related to reduced LPL activity via N-terminal ANGPTL4 and, accordingly, that the ascites in *Angptl4*^{-/-} mice fed a high fat diet is directly connected to enhanced LPL activity.

Our observation that partial deficiency of ANGPTL4 leads to undesirable clinical consequences in mice suggests that therapeutic approaches that only partially inactivate ANGPTL4 and/or are aimed at whole-body inactivation of ANGPTL4 may still carry the risk of major side effects in humans. By contrast, tissue-specific inactivation, in particular adipose tissue-specific and possibly liver-specific inactivation, of ANGPTL4 holds considerably more promise for improving dyslipidemia and reducing coronary artery disease risk without leading to deleterious side-effects (34).


In line with a predominant role of ANGPTL4 in lipid metabolism during fasting, plasma levels of triglycerides, cholesterol, and NEFAs were lower in *Angptl4*^{-/-} mice compared with WT mice specifically in the fasted but not the fed state. Interestingly, in the fasted state, plasma triglyceride, cholesterol, and NEFA levels were similar in *Angptl4*^{hyp} and *Angptl4*^{-/-} mice, which was accompanied by similar levels of LPL protein in the adipose tissue. Accordingly, the expression of low levels of N-terminal ANGPTL4 does not influence LPL protein levels in the fasted state. By contrast, in the fed state, LPL protein levels in adipose tissue were lower in *Angptl4*^{hyp} mice than in *Angptl4*^{-/-} mice, suggesting that a low level of N-terminal ANGPTL4 decreases LPL protein, likely by promoting LPL degradation. The reason why N-terminal ANGPTL4 in *Angptl4*^{hyp} mice has a more pronounced effect on LPL in the fed state than in the fasted state is unclear. Why fasting fails to alter *Angptl4* mRNA in *Angptl4*^{hyp} mice is also unclear. It can be hypothesized that it is due to a disrupted transcriptional regulation by the glucocorticoid receptor via exon 7, as this mechanism is responsible for the induction of *Angptl4* expression by fasting in WT adipose tissue (49, 50). Despite the minimal effect of fasting on levels of N-terminal ANGPTL4 in *Angptl4*^{hyp} mice, LPL protein levels increased, suggesting an additional regulatory mechanism of LPL protein.

In addition to regulating plasma lipid levels, recent reports also suggest a role of ANGPTL4 in glucose homeostasis (51). Using different models, ANGPTL4 deficiency in mice was found to lead to improved glucose tolerance. Consistent with the study by Gusarova et al. (52), we found that *Angptl4*^{-/-} mice chronically fed a high fat diet have drastically lower basal plasma glucose levels and improved glucose tolerance. However, these mice have numerous clinical abnormalities, which prohibit any conclusion on the direct effect of ANGPTL4 deficiency on glucose homeostasis. *Angptl4*^{hyp} mice fed a high fat diet showed a much milder clinical phenotype, concomitant with a more modest yet statistically significant improvement in glucose tolerance; yet acute-phase protein levels were still elevated compared with WT mice. This observation again makes it difficult to derive a solid conclusion on the direct effect of ANGPTL4 deficiency on glucose homeostasis. We previously found that *Angptl4*^{-/-} mice fed a diet high in unsaturated fat, which does not exhibit any clinical complications, were more glucose tolerant than WT mice fed the same diet (53). In addition, it was shown that adipocyte-specific ANGPTL4-deficient mice have markedly improved glucose and insulin tolerance after 1 month and to a lesser extent after five months of high fat feeding, which was suggested to be due to LPL-mediated redistribution of ectopic fat stores to adipose tissue (34). While growing evidence thus connects ANGPTL4 with glucose homeostasis, further studies are necessary to delineate potential mechanisms.

Another interesting question concerns the significance of the lipid-laden Touton giant cells for the onset of the debilitating side effects after high fat feeding. A causal role had been previously questioned by the observation that *Angptl4*^{-/-} mice fed a diet high in *trans* fatty acids develop Touton cells but do not show elevated systemic inflammation or ascites and survive the intervention (30). Here, we found that *Angptl4*^{hyp} mice fed a regular high fat diet, despite showing a much milder inflammation and ascites than *Angptl4*^{-/-} mice, carried similar numbers of Touton giant cells in their mesenteric lymph nodes. These data reinforce the notion that the formation of lipid-laden Touton giant cells is uncoupled from activation of an acute-phase response and chylous ascites (30).

Two previous publications have used the *Angptl4*^{hyp} mice to generate floxed *Angptl4* mice, which in turn were used to generate adipocyte- or brown fat-specific ANGPTL4-deficient mice (33, 34). Deficiency of ANGPTL4 was shown by dramatically reduced qPCR-based amplification of introns 4–5, which covers the region removed by Cre-mediated excision. No information was presented on ANGPTL4 protein levels. Based on our results and calculations, it is possible that in both mouse models there is still significant expression of a truncated N-terminal ANGPTL4 protein derived from exons 1–3 containing the LPL-inhibitory domain. It can be argued that this truncated ANGPTL4 might influence the metabolic phenotype.

In conclusion, we found that ANGPTL4 deficiency increased lipid uptake and respiration in macrophages without affecting LPL protein levels. Furthermore, in comparison to *Angptl4*^{-/-} mice, mice expressing low levels of

N-terminal ANGPTL4 showed a reduced acute-phase response and markedly attenuated chylous ascites following high fat feeding. These findings have significant clinical implications inasmuch as any therapeutic strategy would likely reduce but not completely inactivate ANGPTL4. 

The authors thank Madelene Ericsson and Rakel Nyrén (Department of Medical Biosciences/Physiological Chemistry, Umeå University, Sweden) for their technical assistance with the LPL activity measurements and Imke Vohs (Wageningen University) for her assistance with the H&E staining.

REFERENCES

- Hokanson, J. E., and M. A. Austin. 1996. Plasma triglyceride level is a risk factor for cardiovascular disease independent of high-density lipoprotein cholesterol level: a meta-analysis of population-based prospective studies. *J. Cardiovasc. Risk.* **3**: 213–219.
- Onat, A., I. Sari, M. Yazici, G. Can, G. Hergenç, and G. Ş. Avci. 2006. Plasma triglycerides, an independent predictor of cardiovascular disease in men: A prospective study based on a population with prevalent metabolic syndrome. *Int. J. Cardiol.* **108**: 89–95.
- Sandesara, P. B., S. S. Virani, S. Fazio, and M. D. Shapiro. 2019. The forgotten lipids: triglycerides, remnant cholesterol, and atherosclerotic cardiovascular disease risk. *Endocr. Rev.* **40**: 537–557.
- Goldberg, I. J., R. H. Eckel, and R. McPherson. 2011. Triglycerides and heart disease: still a hypothesis? *Arterioscler. Thromb. Vasc. Biol.* **31**: 1716–1725.
- Kersten, S. 2014. Physiological regulation of lipoprotein lipase. *Biochim. Biophys. Acta.* **1841**: 919–933.
- Davies, B. S. J., A. P. Beigneux, R. H. Barnes, Y. Tu, P. Gin, M. M. Weinstein, C. Nobumori, R. Nyrén, I. Goldberg, G. Olivecrona, et al. 2010. GPIHBP1 is responsible for the entry of lipoprotein lipase into capillaries. *Cell Metab.* **12**: 42–52.
- Beigneux, A. P., K. Miyashita, M. Ploug, D. J. Blom, M. Ai, M. F. Linton, W. Khovidhunkit, R. Dufour, A. Garg, M. A. McMahon, et al. 2017. Autoantibodies against GPIHBP1 as a cause of hypertriglyceridemia. *N. Engl. J. Med.* **376**: 1647–1658.
- Goulbourne, C. N., P. Gin, A. Tatar, C. Nobumori, A. Hoenger, H. Jiang, C. R. M. Grovenor, O. Adeyo, J. D. Esko, I. J. Goldberg, et al. 2014. The GPIHBP1-LPL complex is responsible for the margination of triglyceride-rich lipoproteins in capillaries. *Cell Metab.* **19**: 849–860.
- Conklin, D., D. Gilbertson, D. W. Taft, M. F. Maurer, T. E. Whitmore, D. L. Smith, K. M. Walker, L. H. Chen, S. Wattler, M. Nehls, et al. 1999. Identification of a mammalian angiopoietin-related protein expressed specifically in liver. *Genomics.* **62**: 477–482.
- Kim, I., H. G. Kim, H. Kim, H. H. Kim, S. K. Park, C. S. Uhm, Z. H. Lee, and G. Y. Koh. 2000. Hepatic expression, synthesis and secretion of a novel fibrinogen/angiopoietin-related protein that prevents endothelial-cell apoptosis. *Biochem. J.* **346**: 603–610.
- Kersten, S., S. Mandard, N. S. Tan, P. Escher, D. Metzger, P. Chambon, F. J. Gonzalez, B. Desvergne, and W. Wahli. 2000. Characterization of the fasting-induced adipose factor FIAF, a novel peroxisome proliferator-activated receptor target gene. *J. Biol. Chem.* **275**: 28488–28493.
- Yoon, J. C., T. W. Chickering, E. D. Rosen, B. Dussault, Y. Qin, A. Soukas, J. M. Friedman, W. E. Holmes, and B. M. Spiegelman. 2000. Peroxisome proliferator-activated receptor gamma target gene encoding a novel angiopoietin-related protein associated with adipose differentiation. *Mol. Cell. Biol.* **20**: 5343–5349.
- Zhang, R. 2012. Lipasin, a novel nutritionally-regulated liver-enriched factor that regulates serum triglyceride levels. *Biochem. Biophys. Res. Commun.* **424**: 786–792.
- Quagliarini, F., Y. Wang, J. Kozlitina, N. V. Grishin, R. Hyde, E. Boerwinkle, D. M. Valenzuela, A. J. Murphy, J. C. Cohen, and H. H. Hobbs. 2012. Atypical angiopoietin-like protein that regulates ANGPTL3. *Proc. Natl. Acad. Sci. USA.* **109**: 19751–19756.
- Ren, G., J. Y. Kim, and C. M. Smas. 2012. Identification of RIFL, a novel adipocyte-enriched insulin target gene with a role in lipid metabolism. *Am. J. Physiol. Endocrinol. Metab.* **303**: E334–E351.
- Chi, X., E. C. Britt, H. W. Shows, A. J. Hjelmaas, S. K. Shetty, E. M. Cushing, W. Li, A. Dou, R. Zhang, and B. S. J. Davies. 2017.

- ANGPTL8 promotes the ability of ANGPTL3 to bind and inhibit lipoprotein lipase. *Mol. Metab.* **6**: 1137–1149.
17. Haller, J. F., I. J. Mintah, L. M. Shihanian, P. Stevis, D. Buckler, C. A. Alexa-Braun, S. Kleiner, S. Banfi, J. C. Cohen, H. H. Hobbs, et al. 2017. ANGPTL8 requires ANGPTL3 to inhibit lipoprotein lipase and plasma triglyceride clearance. *J. Lipid Res.* **58**: 1166–1173.
 18. Köster, A., Y. B. Chao, M. Mosior, A. Ford, P. A. Gonzalez-DeWhitt, J. E. Hale, D. Li, Y. Qiu, C. C. Fraser, D. D. Yang, et al. 2005. Transgenic angiotensin-like (Angptl)4 overexpression and targeted disruption of Angptl4 and Angptl3: regulation of triglyceride metabolism. *Endocrinology.* **146**: 4943–4950.
 19. Lichtenstein, L., J. F. P. Berbée, S. J. Van Dijk, K. W. Van Dijk, A. Bensadoun, I. P. Kema, P. J. Voshol, M. Müller, P. C. N. Rensen, and S. Kersten. 2007. Angptl4 upregulates cholesterol synthesis in liver via inhibition of LPL- and HGL-dependent hepatic cholesterol uptake. *Arterioscler. Thromb. Vasc. Biol.* **27**: 2420–2427.
 20. Abid, K., T. Trimeche, D. Mili, M. A. Msolli, I. Trabelsi, S. Nouira, and A. Kenani. 2016. ANGPTL4 variants E40K and T266M are associated with lower fasting triglyceride levels and predicts cardiovascular disease risk in type 2 diabetic Tunisian population. *Lipids Health Dis.* **15**: 63.
 21. Dewey, F. E., V. Gusarova, C. O'Dushlaine, O. Gottesman, J. Trejos, C. Hunt, C. V. Van Hout, L. Habegger, D. Buckler, K.-M. V. Lai, et al. 2016. Inactivating variants in ANGPTL4 and risk of coronary artery disease. *N. Engl. J. Med.* **374**: 1123–1133.
 22. Mandard, S., F. Zandbergen, E. Van Straten, W. Wahli, F. Kuipers, M. Müller, and S. Kersten. 2006. The fasting-induced adipose factor/angiotensin-like protein 4 is physically associated with lipoproteins and governs plasma lipid levels and adiposity. *J. Biol. Chem.* **281**: 934–944.
 23. Dijk, W., and S. Kersten. 2016. Regulation of lipid metabolism by angiotensin-like proteins. *Curr. Opin. Lipidol.* **27**: 249–256.
 24. Mysling, S., K. K. Kristensen, M. Larsson, O. Kovrov, A. Bensadoun, T. J. D. Jørgensen, G. Olivecrona, S. G. Young, and M. Ploug. 2016. The angiotensin-like protein angptl4 catalyzes unfolding of the hydrolase domain in lipoprotein lipase and the endothelial membrane protein gp1hbp1 counteracts this unfolding. *eLife.* **5**: e20958.
 25. Sukonina, V., A. Lookene, T. Olivecrona, and G. Olivecrona. 2006. Angiotensin-like protein 4 converts lipoprotein lipase to inactive monomers and modulates lipase activity in adipose tissue. *Proc. Natl. Acad. Sci. USA.* **103**: 17450–17455.
 26. Dijk, W., P. M. M. Ruppert, L. J. Oost, and S. Kersten. 2018. Angiotensin-like 4 promotes the intracellular cleavage of lipoprotein lipase by PCSK3/furin in adipocytes. *J. Biol. Chem.* **293**: 14134–14145.
 27. Dijk, W., A. P. Beigneux, M. Larsson, A. Bensadoun, S. G. Young, and S. Kersten. 2016. Angiotensin-like 4 (ANGPTL4) promotes intracellular degradation of lipoprotein lipase in adipocytes. *J. Lipid Res.* **57**: 1670–1683.
 28. Desai, U., E. C. Lee, K. Chung, C. Gao, J. Gay, B. Key, G. Hansen, D. Machajewski, K. A. Platt, A. T. Sands, et al. 2007. Lipid-lowering effects of anti-angiotensin-like 4 antibody recapitulate the lipid phenotype found in angiotensin-like 4 knockout mice. *Proc. Natl. Acad. Sci. USA.* **104**: 11766–11771.
 29. Lichtenstein, L., F. Mattijssen, N. J. de Wit, A. Georgiadi, G. J. Hooiveld, R. van der Meer, Y. He, L. Qi, A. Köster, J. T. Tamsma, et al. 2010. Angptl4 protects against severe proinflammatory effects of saturated fat by inhibiting fatty acid uptake into mesenteric lymph node macrophages. *Cell Metab.* **12**: 580–592.
 30. Oteng, A.-B., A. Bhattacharya, S. Brodessa, L. Qi, N. S. Tan, and S. Kersten. 2017. Feeding Angptl4^{-/-} mice trans fat promotes foam cell formation in mesenteric lymph nodes without leading to ascites. *J. Lipid Res.* **58**: 1100–1113.
 31. Dijk, W., M. Heine, L. Vergnes, M. R. Boon, G. Schaart, M. K. C. Hesselink, K. Reue, W. D. van Marken Lichtenbelt, G. Olivecrona, P. C. N. Rensen, et al. 2015. ANGPTL4 mediates shuttling of lipid fuel to brown adipose tissue during sustained cold exposure. *eLife.* **4**: 1–23.
 32. Skarnes, W. C., B. Rosen, A. P. West, M. Koutsourakis, W. Bushell, V. Iyer, A. O. Mujica, M. Thomas, J. Harrow, T. Cox, et al. 2011. A conditional knockout resource for the genome-wide study of mouse gene function. *Nature.* **474**: 337–342.
 33. Singh, A. K., B. Aryal, B. Chaube, N. Rotllan, L. Varela, T. L. Horvath, Y. Suárez, and C. Fernández-Hernando. 2018. Brown adipose tissue derived ANGPTL4 controls glucose and lipid metabolism and regulates thermogenesis. *Mol. Metab.* **11**: 59–69.
 34. Aryal, B., A. K. Singh, X. Zhang, L. Varela, N. Rotllan, L. Goedeke, B. Chaube, J.-P. Camporez, D. F. Vatner, T. L. Horvath, et al. 2018. Absence of ANGPTL4 in adipose tissue improves glucose tolerance and attenuates atherogenesis. *JCI Insight.* **3**: 97918.
 35. Kroupa, O., E. Vorrjö, R. Stienstra, F. Mattijssen, S. K. Nilsson, S. Kersten, G. Olivecrona, and T. Olivecrona. 2012. Linking nutritional regulation of Angptl4, Gp1hbp1, and Lmfl1 to lipoprotein lipase activity in rodent adipose tissue. *BMC Physiol.* **12**: 13.
 36. Markwell, M. A. K., S. M. Haas, L. L. Bieber, and N. E. Tolbert. 1978. A modification of the Lowry procedure to simplify protein determination in membrane and lipoprotein samples. *Anal. Biochem.* **87**: 206–210.
 37. Bolstad, B. M., R. A. Irizarry, M. Astrand, and T. P. Speed. 2003. A comparison of normalization methods for high density oligonucleotide array data based on variance and bias. *Bioinformatics.* **19**: 185–193.
 38. Irizarry, R. A., B. Hobbs, F. Collin, Y. D. Beazer-Barclay, K. J. Antonellis, U. Scherf, and T. P. Speed. 2003. Exploration, normalization, and summaries of high density oligonucleotide array probe level data. *Biostatistics.* **4**: 249–264.
 39. Dai, M., P. Wang, A. D. Boyd, G. Kostov, B. Athey, E. G. Jones, W. E. Bunney, R. M. Myers, T. P. Speed, H. Akil, et al. 2005. Evolving gene/transcript definitions significantly alter the interpretation of GeneChip data. *Nucleic Acids Res.* **33**: e175.
 40. Robblee, M. M., C. C. Kim, J. P. Abate, M. Valdearcos, K. L. M. Sandlund, M. K. Shenoy, R. Volmer, T. Iwawaki, and S. K. Koliwad. 2016. Saturated fatty acids engage an IRE1 α -dependent pathway to activate the NLRP3 inflammasome in myeloid cells. *Cell Reports.* **14**: 2611–2623.
 41. Weinstein, M. M., L. Yin, A. P. Beigneux, B. S. Davies, P. Gin, K. Estrada, K. Melford, J. R. Bishop, J. D. Esko, G. M. Dallinga-Thie, et al. 2008. Abnormal patterns of lipoprotein lipase release into the plasma in GPIHBP1-deficient mice. *J. Biol. Chem.* **283**: 34511–34518.
 42. Mandard, S., F. Zandbergen, S. T. Nguan, P. Escher, D. Patsouris, W. Koenig, R. Kleemann, A. Bakker, F. Veenman, W. Wahli, et al. 2004. The direct peroxisome proliferator-activated receptor target fasting-induced adipose factor (FIAT/PGAR/ANGPTL4) is present in blood plasma as a truncated protein that is increased by fenofibrate treatment. *J. Biol. Chem.* **279**: 34411–34420.
 43. Doolittle, M. H., O. Ben-Zeev, J. Elovson, D. Martin, and T. G. Kirchgessner. 1990. The response of lipoprotein lipase to feeding and fasting. *J. Biol. Chem.* **265**: 4570–4577.
 44. Yoshida, K., T. Shimizugawa, M. Ono, and H. Furukawa. 2002. Angiotensin-like protein 4 is a potent hyperlipidemia-inducing factor in mice and inhibitor of lipoprotein lipase. *J. Lipid Res.* **43**: 1770–1772.
 45. Georgiadi, A., Y. Wang, R. Stienstra, N. Tjeerdema, A. Janssen, A. Stalenhof, J. A. van der Vliet, A. de Roos, J. T. Tamsma, J. W. Smit, et al. 2013. Overexpression of angiotensin-like protein 4 protects against atherosclerosis development. *Arterioscler. Thromb. Vasc. Biol.* **33**: 1529–1537.
 46. Aryal, B., N. Rotllan, E. Araldi, C. M. Ramírez, S. He, B. G. Chousterman, A. M. Fenn, A. Wanschel, J. Madrigal-Matute, N. Warrier, et al. 2016. ANGPTL4 deficiency in haematopoietic cells promotes monocyte expansion and atherosclerosis progression. *Nat. Commun.* **7**: 12313.
 47. Cupp, M., A. Bensadoun, and K. Melford. 1987. Heparin decreases the degradation rate of lipoprotein lipase in adipocytes. *J. Biol. Chem.* **262**: 6383–6388.
 48. He, P. P., T. Jiang, X. P. OuYang, Y. Q. Liang, J. Q. Zou, Y. Wang, Q. Q. Shen, L. Liao, and X. L. Zheng. 2018. Lipoprotein lipase: biosynthesis, regulatory factors, and its role in atherosclerosis and other diseases. *Clin. Chim. Acta.* **480**: 126–137.
 49. Koliwad, S. K., T. Kuo, L. E. Shipp, N. E. Gray, F. Backhed, A. Y. L. So, R. V. Farese, and J. C. Wang. 2009. Angiotensin-like 4 (ANGPTL4, fasting-induced adipose factor) is a direct glucocorticoid receptor target and participates in glucocorticoid-regulated triglyceride metabolism. *J. Biol. Chem.* **284**: 25593–25601.
 50. Gray, N. E., L. N. Lam, K. Yang, A. Y. Zhou, S. Koliwad, and J. C. Wang. 2012. Angiotensin-like 4 (Angptl4) protein is a physiological mediator of intracellular lipolysis in murine adipocytes. *J. Biol. Chem.* **287**: 8444–8456.
 51. Davies, B. S. J. 2018. Can targeting ANGPTL proteins improve glucose tolerance? *Diabetologia.* **61**: 1277–1281.
 52. Gusarova, V., C. O'Dushlaine, T. M. Teslovich, P. N. Benotti, T. Mirshahi, O. Gottesman, C. V. Van Hout, M. F. Murray, A. Mahajan, J. B. Nielsen, et al. 2018. Genetic inactivation of ANGPTL4 improves glucose homeostasis and is associated with reduced risk of diabetes. *Nat. Commun.* **9**: 2252.
 53. Janssen, A. W. F., S. Katiraei, B. Bartosinska, D. Eberhard, K. W. Van Dijk, and S. Kersten. 2018. Loss of angiotensin-like 4 (ANGPTL4) in mice with diet-induced obesity uncouples visceral obesity from glucose intolerance partly via the gut microbiota. *Diabetologia.* **61**: 1447–1458.